Title

Single-cell visualization and quantification of trace metals in Chlamydomonas lysosome-related organelles

Journal

Proceedings of the National Academy of Sciences of the United States of America, 118(16)

ISSN

0027-8424

Authors

Schmollinger, Stefan
Chen, Si
Strenkert, Daniela
et al.

Publication Date

2021-04-20

DOI

10.1073/pnas.2026811118

Peer reviewed

Single-cell visualization and quantification of trace metals in *Chlamydomonas* lysosome-related organelles

Stefan Schmollinger[a,b,c,d], Si Chen[e], Daniela Strenkert[a,b,c], Colleen Hui[a,c,f], Martina Ralle[g], and Sabeeha S. Merchant[a,b,c,d,h,1]

[a]California Institute for Quantitative Biosciences, University of California, Berkeley, CA 94720; [b]Department of Molecular and Cell Biology, University of California, Berkeley, CA 94720; [c]Department of Chemistry and Biochemistry, University of California, Los Angeles, CA 90095; [d]Institute for Genomics and Proteomics, University of California, Los Angeles, CA 90095; [e]Advanced Photon Source, Argonne National Laboratory, Argonne, IL 60439; [f]Physical and Life Sciences Directorate, Lawrence Livermore National Laboratory, Livermore, CA 94550; [g]Molecular and Medical Genetics Department, Oregon Health and Sciences University, Portland, OR 97239; and [h]Department of Plant and Microbial Biology, University of California, Berkeley, CA 94720

Contributed by Sabeeha S. Merchant, March 10, 2021 (sent for review December 17, 2020; reviewed by Caryn E. Outten and Amy E. Palmer)

The acidocalcisome is an acidic organelle in the cytosol of eukaryotes, defined by its low pH and high calcium and polyphosphate content. It is visualized as an electron-dense object by transmission electron microscopy (TEM) or described with mass spectrometry (MS)–based imaging techniques or multimodal X-ray fluorescence microscopy (XFM) based on its unique elemental composition. Compared with MS-based imaging techniques, XFM offers the additional advantage of absolute quantification of trace metal content, since sectioning of the cell is not required and metabolic states can be preserved rapidly by either vitrification or chemical fixation. We employed XFM in *Chlamydomonas reinhardtii* to determine single-cell and organelle trace metal quotas within algal cells in situations of trace metal overaccumulation (Fe and Cu). We found up to 70% of the cellular Cu and 80% of Fe sequestered in acidocalcisomes in these conditions and identified two distinct populations of acidocalcisomes, defined by their unique trace elemental makeup. We utilized the *vtc1* mutant, defective in polyphosphate synthesis and failing to accumulate Ca, to show that Fe sequestration is not dependent on either. Finally, quantitation of the Fe and Cu contents of individual cells and compartments via XFM, over a range of cellular metal quotas created by nutritional and genetic perturbations, indicated excellent correlation with bulk data from corresponding cell cultures, establishing a framework to distinguish the nutritional status of single cells.

vacuole VTC XRF | trace metal sequestration | heavy metal detoxification

Trace metals like iron (Fe), copper (Cu), manganese (Mn), and zinc (Zn) play a crucial role as cofactors, providing a range of chemical capabilities to enzymes central to life. Metals also provide structural stability to proteins (1, 2) and enable the catalysis of essential metabolic reactions by providing functional groups that are not readily available via the side chains of amino acids. Consequently, trace metals are required in ∼40% of all enzymes as part of their catalytic centers (3, 4). Individual enzymes are often optimized to utilize a specific metal cofactor, with respect to the chemical utility of that particular trace metal for the catalyzed reaction, the metal's specific requirements for the binding site in the protein (dimensions, charge, coordination preferences), and the availability of the trace metal within the organism's reach. There is, however, the possibility of mismetalation, largely attributed to protein structural flexibility and somewhat similar ionic radii and coordination preferences of first-row trace metals (5, 6). Enzyme mismetalation can harm the cell directly by loss of function (7, 8), by accumulation of unintended products, or by the production of toxic side products, for example, reactive oxygen species (9). Cells have therefore developed elaborate strategies to facilitate correct metalation, including preassembling metal cofactors (which allows for easier distinction and delivery of specific metals), the use of metallochaperones (removing especially thermodynamically favored elements like Cu/Zn from the accessible, intracellular trace metal pool), and the compartmentalization of trace metal metabolism (adjusting metal concentrations locally in order to direct binding to target proteins) (6, 10, 11).

Chlamydomonas reinhardtii is a unicellular green alga that has been widely used as a eukaryotic, photosynthetic reference system, and therefore exploited in our laboratory to study trace metal metabolism. It has a short generation time (∼6 h), is a facultative heterotroph, and can be grown to high densities (12). *Chlamydomonas* requires a broad spectrum of metal cofactors to sustain its photosynthetic, respiratory, and metabolic capabilities, with Fe, Cu, Mn, and Zn as the major first-row trace metals involved in these processes. In the last 20 y, studies have revealed a repertoire of assimilatory and distributive transporters in *Chlamydomonas*, using biochemical and genomics approaches (13–17), discovered mechanisms for metal sparing and recycling to ensure economy (18–21), and identified metal storage sites (2, 22–24).

Storage sites are crucial components of trace metal homeostasis. The capacity to sequester individual trace metals is important for controlling protein metalation, detoxification in situations of overload, and buffering during metabolic remodeling. Metal storage provides a selective advantage in competitive environments when transition metals are scarce. One well-known storage site is ferritin, a soluble, mostly cytosolic (animals) or mostly plastidic (plants), 24-subunit oligomer that can oxidize ferrous to ferric Fe and store up to ∼4,500 ferric ions in mineralized form in its core (25, 26). The importance of ferritin as an Fe store is well documented in

Significance

Transition metals are of crucial importance for primary productivity; their scarcity limits crop yield in agriculture and carbon sequestration on a global scale. Copper (Cu), iron (Fe), and manganese (Mn) are among the most important trace elements that enable the redox chemistry in oxygenic photosynthesis. The single-celled, eukaryotic green alga *Chlamydomonas reinhardtii* is a choice experimental system for studying trace metal homeostasis in the context of phototrophy, offering all the advantages of a classical microbial system with a well-characterized photosystem and trace metal metabolism machinery of relevance to plants. This project identifies and differentiates different trace metal storage sites in *Chlamydomonas* and uncovers the dynamics of trace metal storage and mobilization in situations of fluctuating resources.

Author contributions: S.S., M.R., and S.S.M. designed research; S.S., S.C., D.S., C.H., and M.R. performed research; S.S., S.C., and M.R. analyzed data; and S.S. and S.S.M. wrote the paper.

Reviewers: C.E.O., University of South Carolina; and A.E.P., University of Colorado Boulder.

The authors declare no competing interest.

[1]To whom correspondence may be addressed. Email: sabeeha@berkeley.edu.

This article contains supporting information online at https://www.pnas.org/lookup/suppl/doi:10.1073/pnas.2026811118/-/DCSupplemental.

Published April 16, 2021.

eukaryotes. In *Chlamydomonas*, the pattern of expression of ferritin is more consistent with a role in buffering Fe during metabolic transitions, for example from phototrophy to heterotrophy during Fe starvation (23, 27). Vacuoles, lysosome-related, and other acidic organelles, are equally important storage organelles in eukaryotes (28–33). In yeast and plants, these organelles can sequester metals for future use (34). Chlorophyte algae employ a set of smaller cytosolic vacuoles, including contractile vacuoles and acidocalcisomes. Contractile vacuoles (CVs) manage the water content in the cytoplasm; in a fresh water alga that is predominantly facing hypotonic environments (35, 36), water is removed from the cell, potentially using potassium (K) and/or chloride (Cl) (37) to generate an osmotic gradient to attract water to the CV. Acidocalcisomes are lysosome-related organelles in the cytosol, defined by their low pH and high levels of calcium and polyphosphate (polyP) content (38, 39). In *Chlamydomonas* and other green algae this organelle may also contain K (40, 41). Acidocalcisomes can be identified as electron-dense granules by transmission electron microscopy (TEM) or by utilizing specific probes targeting either the low pH environment or the specific elemental makeup of the compartment (24, 42–44). In addition, acidocalcisomes have been visualized using their unique elemental signature by mass spectrometry (MS)-based imaging techniques, specifically nanoscale secondary ion mass spectrometry (nanoSIMS), or X-ray fluorescence microscopy (XFM) (45, 46). These methods demonstrated that, at least in *Chlamydomonas*, the acidocalcisome can house high amounts of Cu and Mn in excess conditions (24, 47), making it a prime candidate for Fe storage as well.

XFM is a synchrotron-based technique that utilizes X-rays to produce photons in the object to be visualized. The energies of these fluorescent photons are element specific and can be used to determine elemental distribution and concentrations in whole cells or subcellular compartments (48–50). High energy X-rays (>10 keV) penetrate biological material deep enough so that no sectioning is required. True elemental distributions are obtained when metabolic states are preserved rapidly using either vitrification or chemical fixation. XFM has previously been utilized to determine the elemental content of vacuoles of phagocytes infected with various *Mycobacterium* species (51), to demonstrate transient zinc relocation to the nucleus during macrophage differentiation (52) and the mobilization of Cu during angiogenesis (53).

In this work, we employed XFM with sub-100-nm spatial resolution to identify an Fe storage site in *Chlamydomonas*, determine the spatial distribution of multiple essential trace elements in chlorophyte algae, and quantify acidocalcisomal metal content in single cells in situations of Fe and Cu overaccumulation. We took advantage of a *Chlamydomonas* vacuolar transporter chaperone (*vtc1*) mutant (defective in polyP synthesis and hence also Ca content) (43, 47) to distinguish the role of polyP and Ca in acidocalcisome Fe sequestration. XFM also enabled the comparison of single-cell trace metal quotas with bulk quantification of Cu and Fe in corresponding cell cultures, allowing us to distinguish the nutritional state for Cu and Fe in individual cells.

Results

XFM Is an Excellent Technique to Visualize Trace Metal Sequestration in Microalgae. We first focused on Zn deficiency in *Chlamydomonas*, where cells overaccumulate intracellular Cu, since this condition offers excellent signal to noise, and the site of Cu(I) accumulation was already identified as the acidocalcisome (15, 24). Tandem inductively coupled plasma mass spectrometry (ICP-MS/MS) of 5×10^7 *Chlamydomonas* cells collected from Zn-deficient cultures showed that their Zn content was reduced to ~1/3 of the abundance compared with cells grown in Zn-replete medium (Fig. 1*A*). The Zn-deficient cells had high intracellular Cu content, corresponding to ~20 times the amount found in Zn-replete conditions (Fig. 1*A*), consistent with results from earlier studies in which a similar overaccumulation of Cu was observed when intracellular Zn levels dropped to less than $\sim 1 \times 10^7$ atoms/cell (15). Zn-deficient cells also accumulated Fe, to ~3 times the amount found in replete conditions, while the amount of intracellular P and Ca did not significantly change (Fig. 1*A*). Previously, we showed that Cu is sequestered into distinct Ca-containing foci using a fluorescent probe to identify Cu(I) foci and complementary, direct

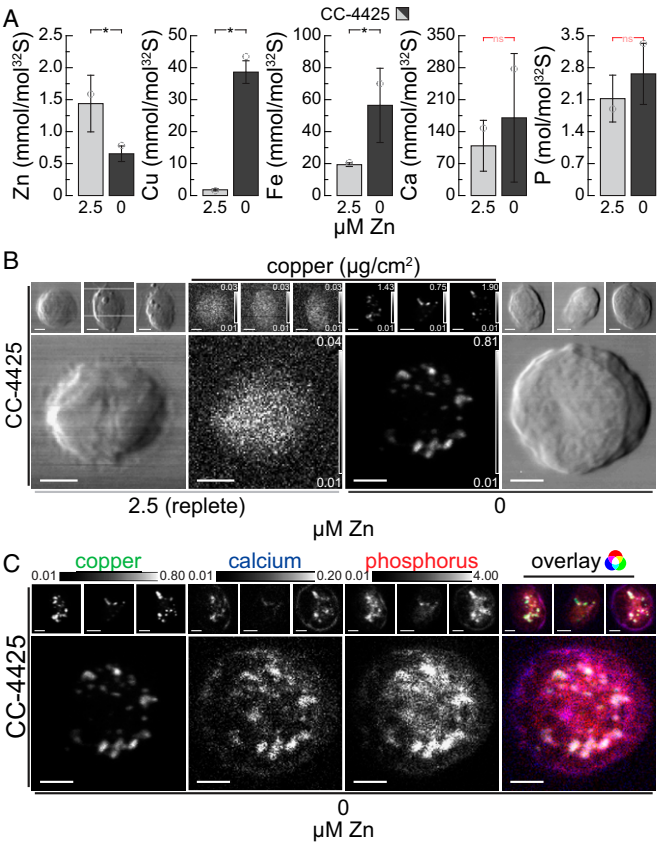

Fig. 1. Zn-deficient cells accumulate copper (Cu), which is sequestered with Ca and P in acidocalcisomes. (*A*) Zn, Cu, Fe, Ca, and P contents of *C. reinhardtii* wild-type strain CC-4425, as measured by ICP-MS/MS, either in the presence of 2.5 μM Zn (replete, light gray), or after two rounds of growth (five generations each) in Zn-deficient growth medium (Zn deficient, dark gray). Elemental content is normalized to total cellular S content as a measure for total biomass; error bars indicate SD of individual cultures ($n \geq 3$); the open circles indicate the elemental content of the specific batch that was used for XFM analysis (B and C). Asterisks indicate significant differences (*t* test, $P \leq 0.05$); nonsignificant (ns) outcomes are indicated in red. (*B*) Cu distribution in four individual CC-4425 wild-type cells, in Zn-replete (*Left*) or Zn-deficient (*Right*) conditions, measured by X-ray fluorescence microscopy at the Bionanoprobe (APS). The images of chemically fixed alga cells show cell outlines (outside panels) and Cu distribution (inside panels) ranging from the minimal (black) to maximal (white) Cu concentration in the individual image (in μg/cm^2). The actual individual minimum and maximum concentration of Cu for each cell are denoted in the *Lower* and *Upper Right* corner of each image, respectively. (Scale bars at *Lower Left*, 2 μm.) The cells were fixed and stored at room temperature; the images were acquired using fly-scan mode (continuous motion in the horizontal direction) at low temperatures with 70-nm step size and 300-ms dwell time per position. The fluorescence maps were created by performing peak area fitting for every position utilizing the MAPS software suite. (*C*) Cu, Ca, and P distribution of the four wild-type cells in Zn deficiency from *B*, as well as the overlay of the three elements. All elemental distributions for all cells are depicted between shared, fixed minimal (black), and maximal (white) elemental concentrations, denoted above the images (in μg/cm^2). (Scale bars at *Bottom Left* of each image, 2 μm.) The *Rightmost* image shows the overlay of the three elements, where Cu contributes the green, Ca the blue, and P the red color.

elemental identification of Ca and Cu by nanoSIMS imaging of thin sections. Noting that elemental maps derived from nanoSIMS are quantified relative to another abundant element in the section, we sought a quantitative description of the organelle utilizing XFM.

Cu displayed different localization patterns in cells grown in Zn-replete vs. Zn-deficient conditions. While Cu was distributed equally throughout the cell in replete conditions, it was found predominantly in foci in Zn deficiency (Fig. 1*B* and *SI Appendix*, Fig. S1*A*) similar to the earlier findings in TEM, nanoSIMS, and fluorescent images. Ca, as described earlier (24), and also P were found to be colocalized with Cu to the foci, both in chemically fixed and vitrified cells (Fig. 1*C* and *SI Appendix*, Fig. S1*B*). In general, vitrified samples had sharper intracellular structures compared with chemically fixed material, which is especially pronounced for P and Ca. Both methods of preservation, however, preserved the Cu sequestration site and maintained the colocalization pattern sufficiently. Colocalization confirmed and further strengthens the conclusion that indeed acidocalcisomes, namely acidic, polyP- and calcium-rich, cytosolic vacuoles, were the storage site for Cu in Zn deficiency. By confirming and extending our earlier findings, we conclude that XFM, using either chemically fixed or vitrified algae, is a viable technique for analyzing intracellular metal storage compartments.

Fe Is Sequestered in *Chlamydomonas* Acidocalcisomes Independently of polyP and Ca. Based on the data presented here and described previously (24, 47), we recognize the acidocalcisome as a prime location for essential metal storage in *Chlamydomonas*. In addition to overaccumulation of Cu in Zn deficiency and Mn in excess Mn environments, we asked if the organelle might also store Fe. Fer1, the major isoform of ferritin in *Chlamydomonas*, was found to be less abundant in cells cultured in medium supplemented with excess Fe, indicating that other storage sites might primarily be used for Fe sequestration in *Chlamydomonas* (23). We used the following strategy to overload *Chlamydomonas* cells with Fe. First we subjected cells to a brief period of Fe limitation (0.1 to 0.25 μM Fe in the medium), in which Fe assimilation components are dramatically up-regulated (17). Accordingly, upon supply of excess Fe (200 μM Fe, corresponding to 10-fold the amount supplied in a replete culture), the cells took up large amounts of Fe (Fig. 2*A* and *SI Appendix*, Fig. S2), resulting in transient overaccumulation of Fe to about 8-fold the amount found in typical replete cultures. Elevated Fe levels persist for about 48 to 72 h, before a lower, but still elevated state (2- to 3-fold relative to a typical replete culture) is reached. The transiently overelevated Fe levels span a period of two to three generations at peak abundance. During this time, Fe needs to be stored safely to avoid detrimental effects from Fe toxicity (8).

In order to analyze the contribution of acidocalcisomes to Fe handling in Fe overaccumulating conditions directly, we analyzed the distribution of Fe in corresponding wild-type cells as well as in the *vtc1* mutant (43). The VTC complex is a multisubunit membrane-spanning enzyme (54, 55) responsible for polyP synthesis in the acidic vacuoles (56, 57). In *Saccharomyces cerevisiae*, among the several proteins of the complex, only loss of VTC1 function results in a complete loss of the entire complex (55). Consistent with VTC1 function and earlier studies (47), *Chlamydomonas vtc1* mutants have reduced total cellular P, ~40% relative to wild-type and the complemented strain (*VTC1-C2*), presumably attributed to reduced acidocalcisomal polyP content (Fig. 2*A* and *SI Appendix*, Fig. S2*B*). Interestingly, elemental analysis also showed a dramatic reduction of cellular Ca in the mutant compared with both the wild-type and complemented strain (Fig. 2*A* and *SI Appendix*, Fig. S2*B*), suggesting that most of the cellular Ca is associated with polyP in acidocalcisomes. Wild-type, *vtc1* mutant, and complemented strain (*VTC1-C2*) showed similar intracellular Fe accumulation (approximately eight times the amount in Fe-replete conditions) after excess Fe addition to Fe-starved cells (Fig. 2*A* and *SI Appendix*, Fig. S2). Furthermore, temporal and concentration-dependent elemental profiles indicated similar behavior of wild-type, mutant, and complemented strains (*SI Appendix*, Fig. S2) upon Fe resupply. In both mutant and wild-type cells, Fe is concentrated into distinct foci in the Fe-overload situation, while at low intracellular Fe levels, the Fe is more evenly distributed throughout the cell (Fig. 2*B*), presumably largely in Fe-binding proteins. According to XFM, Fe foci contained also both Ca and P in wild-type cells, suggesting the acidocalcisome as the likely site of Fe sequestration (Fig. 2*C* and *SI Appendix*, Fig. S3). In the *vtc1* mutant, where acidocalcisomes lack polyP and Ca, the same sequestration pattern was observed (Fig. 2*C* and *SI Appendix*, Fig. S3). Additionally, in wild-type algae but not in the *vtc1* mutant, P accumulates alongside Fe (Fig. 2*A*).

As mentioned above, another situation in which Fe overaccumulates in cells is under Zn starvation, where the Fe content is comparable to cells exposed to long-term Fe excess, approximately two to three times the quota of typical Zn- and Fe-replete cultures (Figs. 1*A* and 3*A*). When we tested Zn-deficient wild-type and *vtc1* cells for the site of Fe accumulation, we found the same pattern as in the Fe-overload situation. Specifically, a punctate pattern of Fe colocalized with Ca and P in wild-type cells, and no impact of the *vtc1* mutant on the Fe content or pattern of distribution (Fig. 3 *A* and *B*). On the other hand, the *VTC1* genotype did affect Mn overaccumulation in Zn deficiency (Fig. 3*A*) and upon Fe overload (*SI Appendix*, Fig. S2*B*), just as it did in situations of Mn overload (47). Like Fe, Cu accumulation in Zn deficiency was also not impacted by loss of acidocalcisomal polyP synthesis (Fig. 3*A*). In all experiments, Ca and P were reduced in the *vtc1* mutant but restored in the complemented strains, confirming that Ca accumulation requires VTC1 function (Figs. 2*A* and 3*A* and *SI Appendix*, Fig. S2). Taken together, we conclude that overaccumulated Fe, independent of the absolute amount (two- to eightfold), is housed in the acidocalcisome, defined by its Ca and P contents. We further conclude that acidocalcisomal polyP and Ca are not required for Fe accumulation in the organelle, in contrast to Mg and Mn accumulation (47, 58).

Cu and Fe Quota of Single Cells Can Be Determined Accurately Using XFM. Because XFM is element specific and quantitative, we sought to compare intracellular Cu and Fe quotas at single-cell resolution with bulk ICP-MS/MS measurements of 5×10^7 *Chlamydomonas* cells cultured in the same conditions. Our experimental conditions offer a dynamic range of two orders of magnitude with respect to Cu and Fe contents. In multiple XFM analyses, five to eight individual cells were each analyzed in Fe-limited (0.1 μM Fe), Fe-replete (20 μM Fe), Fe-accumulating (Zn deficient, 20 μM Fe, 0 μM Zn), and Fe-overaccumulating (0.1 μM Fe, 200 μM Fe addition) conditions. Data from four experimental runs, over a period of 2 y, are presented here. With the exception of Fe-replete conditions, all growth conditions were measured multiple times from independent experiments or different strains, either rapidly vitrified or chemically fixed. This is reflected by individual data points in the graphs (Fig. 4 *A* and *B*). The total intracellular Fe content in the individual cells, as measured by XFM, correlated well with the intracellular content of the bulk cultures, as measured with ICP-MS/MS (Fig. 4*A*). Quantitative XFM measurements allowed accurate measurement of single-cell Fe content and therefore is indicative of the Fe-nutritional state of an individual cell. For Cu, we analyzed conditions representing three different stages of Cu accumulation: Cu-replete (2 μM Cu), Cu-accumulating (2 μM Cu, 0.1 μM Fe before and after 200 μM Fe addition), and Cu-overaccumulating conditions (2 μM Cu, 0 μM Zn). Similar to Fe, we noted a remarkable correlation ($r^2 > 0.8$) between single-cell and bulk measurements (Fig. 4*B*). Again, XFM on its own allows the distinction between various states of Cu nutrition and accurately assesses the total intracellular content. Quantitative data from both, chemically fixed (solid symbols and errors, Fig. 4 *A* and *B*) and

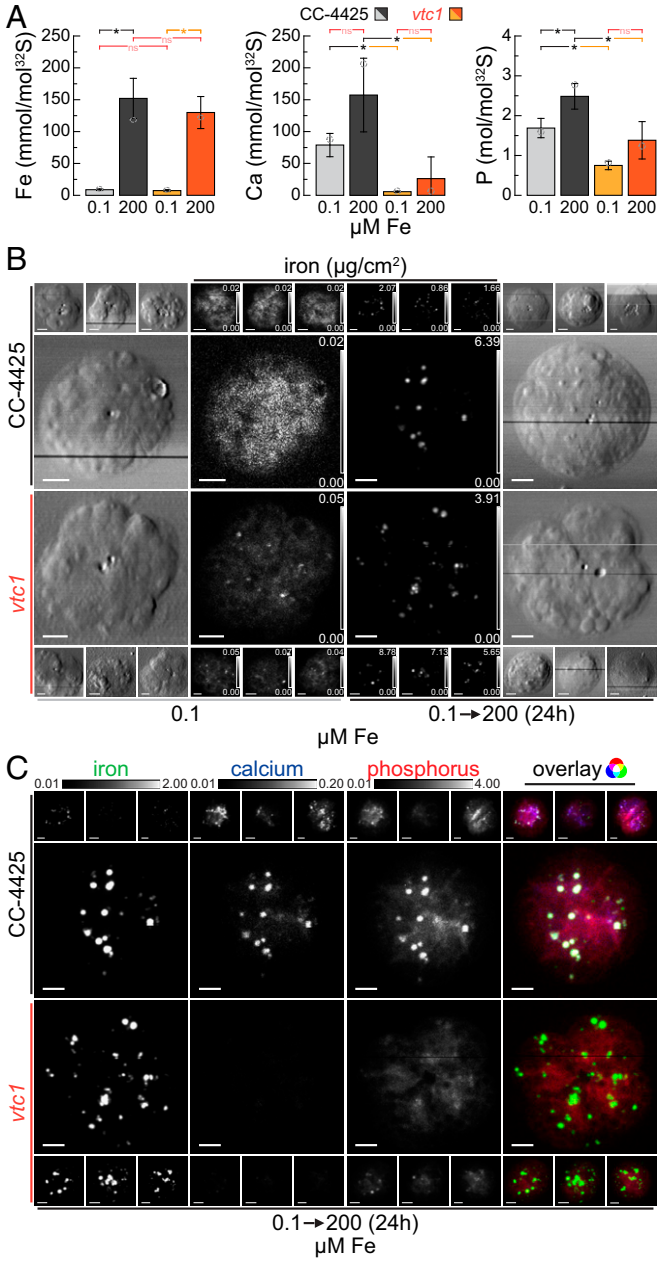

Fig. 2. Acidocalcisomes serve as Fe storage sites during transient overload; vacuolar Ca and polyP is not required for Fe sequestration. (*A*) Total Fe, Ca, and P contents of *C. reinhardtii* wild-type (CC-4425, gray bars) and the *vtc1* mutant strains (orange bars), as measured by ICP-MS/MS, either in Fe-limiting conditions (0.1 µM Fe) or 24 h (two doublings) after the addition of 200 µM Fe to Fe-limited cells (transient Fe overaccumulation). The elemental content is normalized to total cellular S content, as a measure for total biomass; error bars indicate SD of individual cultures ($n \geq 3$); open circles indicate the elemental content of the specific batch used for X-ray fluorescence microscopy analysis in *B* and *C*. Asterisks indicate significant differences (*t* test, $P \leq 0.05$), nonsignificant (ns) outcomes are indicated in red. (*B*) Fe distribution of four individual cells, in Fe-limited conditions or after 24 h of Fe excess, measured by X-ray fluorescence microscopy at the Bionanoprobe (APS). Cells were prepared as described in Fig. 1*B*. The images of chemically fixed alga cells show the cell outlines (outside panels) and the Fe distribution (inside panels) ranging from minimum (black) to maximum (white) Fe concentration in µg/cm^2; actual minimum and maximum concentrations for each cell are noted in the *Lower* and *Upper Right* corner of each image. (Scale bars at *Bottom Left*, 2 µm.) (*C*) Fe, Ca, and P distribution of the eight (four wild type and four mutant) 24-h Fe-excess cells from *B*, as well as overlay. All elemental distributions for all cells are depicted between shared, fixed minimal (black), and maximal (white) elemental concentrations, denoted above the images (in µg/cm^2). (Scale bars at *Bottom Left*, of each image, 2 µm.) The *Rightmost* image shows the overlay of the three elements, where Fe contributes the green, Ca the blue, and P the red color.

vitrified (dashed symbols and errors, Fig. 4 *A* and *B*) samples, were obtained and compared equally well with ICP MS/MS data, both for Fe and Cu content. Synchrotron beamline time allocation is a crucial limiting factor with respect to the number of cells that can be completely scanned at the desired spatial resolution. Similar to other imaging-based techniques, we made an effort to "randomly" choose cells of various sizes for high-resolution imaging, insofar as this was possible with the small number of cells that was analyzed per condition. The size range reflects the size variation in batch cultures from an asynchronous population. This allows us to control for cell-cycle stage-specific dynamics, but it can also contribute to the variance when elemental abundance data are normalized per cell, like in this case. For other elements we did not actively seek to manipulate their intracellular accumulation (Ca and P levels were altered in *vtc1* mutant strains as described above, Mn was accumulating in Zn deficiency to two to three times the amount of replete levels), and therefore their intracellular abundance did not span multiple orders of magnitude. In general P, S, and Ca abundance in individual cells, as measured by XFM, matches the levels measured by ICP-MS/MS. For Mn, the abundance measured by XFM was low, potentially from interference, but the relative content correlates with increasing amounts of intracellular Mn (*SI Appendix*, Fig. S4). For Zn, background levels were too high to allow for a quantitative assessment (Fig. 4*C*). Taken together, we conclude that Fe, P, S, Ca, and Cu levels of individual cells can be accurately quantified using XFM and can be used to predict the nutritional status of single cells in environmental samples. Mn and Zn measurements allowed only for the analysis of spatial distribution and relative changes using the present setup.

S Performs Better than P in Facilitating Comparisons between Bulk Cells and Elemental Distributions. In order to facilitate the comparison between trace metal abundance data acquired by ICP-MS/MS and the spatially distributed XFM data, we explored the possibility of using phosphorus (P) or sulfur (S) for normalization in addition to cell numbers (for bulk elemental content) and cell area (for spatially distributed elemental maps). Both P and S were promising candidates for normalization because both elements' distribution can be accurately analyzed in XFM (59, 60) and accurately quantified with ICP-MS/MS in mass-shift mode (61, 62). Using cellular P or S content for normalization allows us to correct for synchronization artifacts, introduced from experimental perturbations, for example in experiments where high amounts of Fe were added back to Fe-starved cells (*SI Appendix*, Fig. S2*A*, 6-h time point). Additionally, P or S normalization allows us to account for differences in cell size, resulting from random selection of cells of a range of different sizes during XFM analysis. Elemental distribution maps for S or P might also facilitate the analysis of enrichment of elements within storage compartments, when equally distributed they could better reflect depth of the cell at each position of the image, compared with using the area alone (*SI Appendix*, Figs. S2 and S5, also ref. 52).

First, we analyzed the amount of intracellular S and found that it was not affected by the perturbations used in this work (*SI Appendix*, Fig. S2). The total P content in some of the strains used in this study (*vtc1*) was reduced, but P was not affected by the Fe regime (Fig. 2*A* and *SI Appendix*, Fig. S2*B*) or by Zn status (Fig. 3*A*). Consequently, in a single genotype, changes to trace element contents between conditions were not affected by the choice of normalization (P, S, or cell number (*SI Appendix*, Fig. S2*A*). When comparing with biomass, measured as nonpurgeable organic

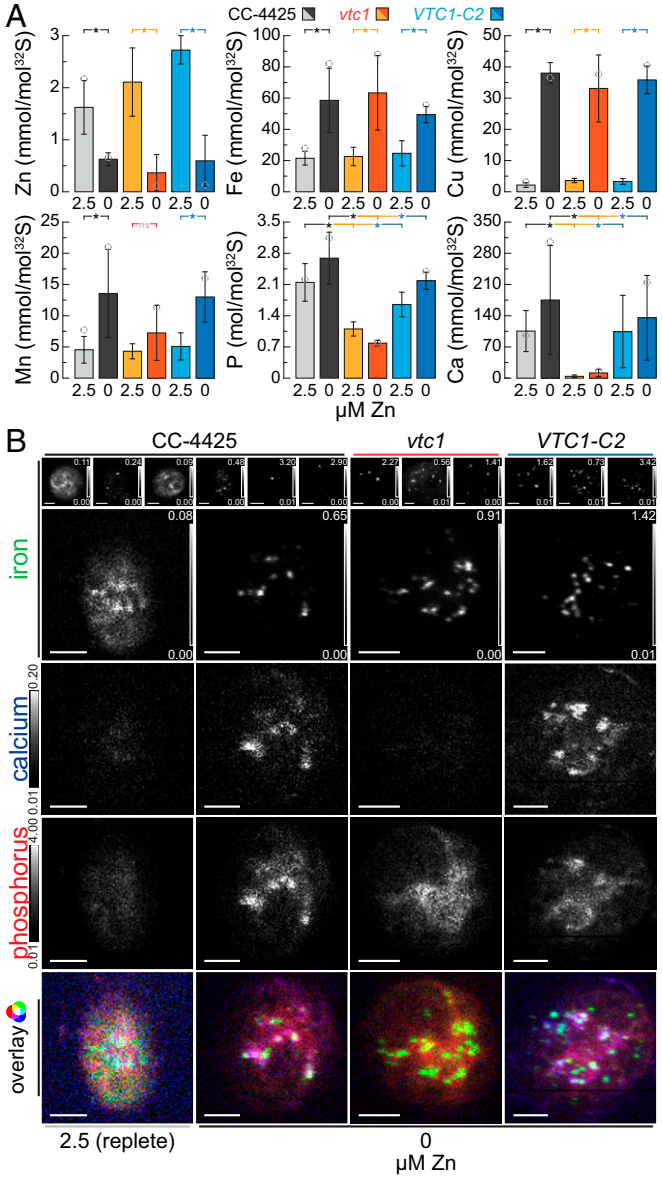

Fig. 3. Fe accumulated in Zn deficiency is sequestered in acidocalcisomes, independent of Ca and polyP. (*A*) Total Zn, Fe, Cu, Mn, Ca, and P contents of *C. reinhardtii* wild-type (CC-4425, gray bars), the *vtc1* mutant (orange bars), and *VTC1-C2* complemented strain (blue bars), as measured by ICP-MS/MS, either in the presence of 2.5 μM Zn (replete, lighter colors) or after two rounds of growth (five generations each) in Zn-deficient growth medium (Zn deficient, darker colors). The elemental content is normalized to total cellular S content, as a measure for total biomass; error bars indicate SD of individual cultures ($n \geq 3$); open circles indicate the elemental content of the specific batch used for X-ray fluorescence microscopy analysis (*B*). Asterisks indicate significant differences (*t* test, $P \leq 0.05$), nonsignificant (ns) outcomes are indicated in red. (*B*) Fe distribution in four individual cells from the wild-type (CC-4425), the *vtc1* mutant, and *VTC1-C2* complemented strain (blue bars) in Zn-replete or Zn-deficient conditions, as measured by X-ray fluorescence microscopy at the Bionanoprobe (APS). Cells were prepared as described in Fig. 1*B*. The minimum (black) to maximum (white) Fe concentration in μg/cm^2 is depicted in the *Lower* and *Upper Right* corner of each image; elemental distributions for Ca and P in all cells are depicted between shared, fixed minimal (black), and maximal (white) elemental concentrations, denoted *Left* of the images (in μg/cm^2). (Scale bars at *Bottom Left*, 2 μm.) The *Bottom* image shows the overlay of the three elements, where Fe contributes the green, Ca the blue, and P the red color.

carbon content (NPOC) (*SI Appendix*, Fig. S5), S content correlated better with the carbon content of cells than did P. S performed equally well in both genotypes for the correlation with biomass (*SI Appendix*, Fig. S5*A*), while for P the correlation improved markedly when *vtc1* was omitted (*SI Appendix*, Fig. S5*B*), although it did not reach to the level of correlation observed for S. We noted also that P (Figs. 1*C*, 2*C*, and 3*B*) was less evenly distributed than S in cells (*SI Appendix*, Fig. S6), in part because of its accumulation in the acidocalcisomes, but also because of segregation in other organelles, including the chloroplast, which appears to have less P compared with other compartments. Taken together, P content varies between strains, exhibits a more complex intracellular distribution and less accurately captures biomass. We conclude that S is a better choice for area-dependent normalization. P does generally correlate well with biomass, leaving the possibility of its use for normalization in a different context.

Two Types of Acidocalcisomes Can Be Distinguished Based on Their Elemental Composition. In order to identify the elemental composition of the compartments that contain overaccumulating trace metals, we used a *k*-means cluster analysis feature in the MAPS software (63) to identify continuous, secluded areas with high Cu or Fe contents in various metal-accumulating conditions. In Zn-deficient cells, as much as 70% (~55% on average) of the intracellular Cu was found in areas containing storage compartments. We found Fe, Ca, P, and Mn to be enriched in these areas, either relative to the cell area or the S content present in these areas (Fig. 5*A*). In Fe-overaccumulating conditions up to 80% (~65% on average) of the total cellular Fe was found in areas containing storage compartments. Again, we found Ca, P, and Mn, but Zn instead of Cu to colocalize with Fe. The concentrations of P and Ca within these areas was comparable between Cu- and Fe-accumulating conditions, while the combined concentration of Fe and Cu in the areas containing storage compartments was ~3-fold higher in Fe-accumulating conditions (Fig. 5*B*). In addition, the metal composition of these areas was significantly different in Cu- and Fe-accumulating conditions. In Zn deficiency, the areas contained mixed trace metal populations of predominantly Fe and Cu, while Fe alone was the dominating metal in Fe-overaccumulating conditions. When analyzing intracellular trace metal abundance outside the metal storage sites (Fig. 5*C*), similar Fe concentrations were maintained between replete, Fe-overaccumulating and Zn-deficient conditions, indicating that excess Fe is successfully sequestered in the acidocalcisomes. Intracellular Fe levels were however reduced ~5-fold in Fe-limited conditions (Fig. 5*C*), indicative of the operation of Fe-sparing responses (19). For Cu on the other hand, in Zn-deficient (copper-accumulating) conditions, intracellular Cu levels outside the acidic vacuoles are also elevated ~10-fold, consistent with an initiating event for Cu accumulation at a cytoplasmic site.

Acidocalcisomes covered ~50% more cellular area in Fe-overaccumulating conditions, compared with Cu-accumulating conditions (Zn deficiency) (Fig. 5*D*). In both conditions despite more such organelles in Fe-accumulating conditions, the average acidocalcisome had a similar radius of ~0.3 μm (Fig. 5*D*). In summary, the size (diameter), Ca and P concentration of acidocalcisomes were retained between the two physiologically distinct metal-accumulating conditions, whereas the number of acidocalcisomes and the abundance and composition of the accumulated material were altered, allowing the cell to accommodate different demands for trace metal sequestration.

Discussion

The acidocalcisome is an acidic vacuole in the cytosol of most eukaryotic organisms, high in polyP and Ca content (42). In *Chlamydomonas*, the organelle is more prevalent when cells reach stationary phase (44) and in situations of nutrient limitation, for example in S deficiency (43), N deficiency (44), and Zn deficiency

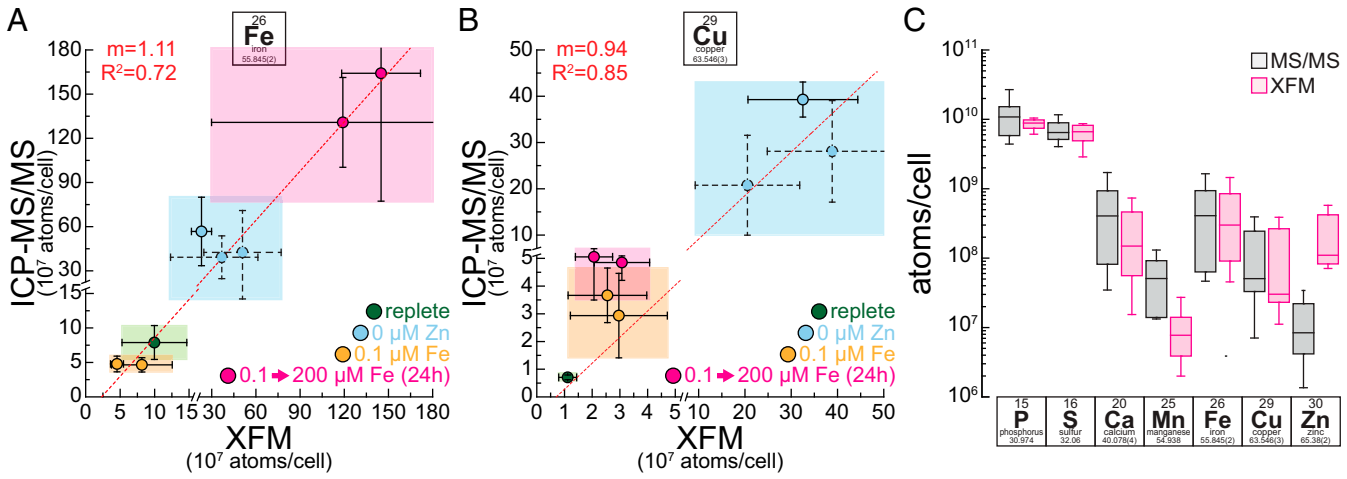

Fig. 4. Single-cell Fe and Cu content accurately recapitulates batch culture data. (*A* and *B*) Correlation of Fe (*A*) and Cu (*B*) content as measured by X-ray fluorescence microscopy (*x* axis) and ICP-MS/MS (*y* axis). Error bars in *x* and *y* direction indicate SD in the measurements between at least four individual cells (XFM) or between at least three independent cultures (ICP-MS/MS). Green areas indicate cells/cultures from replete conditions, blue colored areas indicate Zn-deficient conditions (Cu overaccumulation, Fe two to three times replete levels), pink areas indicate 24 h of Fe excess (Fe overaccumulation, Cu two to four times replete levels), and orange areas indicate Fe-limited conditions (low Fe, Cu two to four times of replete levels). Solid outlines of data points and error bars are associated with chemically fixed samples and dashed outlines with samples that were vitrified. Both axes were broken at the same position to magnify samples with lower intracellular Fe or Cu levels. A linear regression analysis was performed in OriginPro (v9.1); the resulting regression line is presented in the image as a red dashed line, interrupted only from the axis break. R^2 and slope (m) of the analysis are denoted in red in the *Top Left* corner. (*C*) Box plots for elemental content of different intracellular elements, as measured by ICP-MS/MS in between all experimental conditions (gray) and in between all imaged cells in all experimental conditions (pink). From *Bottom* to *Top*, horizontal lines indicate 5%, 25%, 50%, 75%, and 95% quantile.

(24). All of these perturbations are associated with a strong reduction in the growth rate, resulting from the absence of a single, essential nutrient, therefore presenting the opportunity for cells to accumulate other, nonlimiting nutrients in excess amounts. While the role of the acidocalcisome for nutrient storage in N and S deficiency is still unclear, a role in trace metal homeostasis is established. Specifically, it has been demonstrated that Zn-deficient *Chlamydomonas* acidocalcisomes facilitate trace metal storage and harbor excess amounts of other nonlimiting trace elements, most prominently Cu, but also Fe and Mn (Figs. 1 and 3). Nutrients accumulated in these situations are accessible, at least in the case of Cu, which can be later utilized to facilitate growth when Cu becomes limiting (24). More recently, the acidocalcisome was found to store excess Mn, which can also be utilized later (47) and to store excess Fe, when indulged with Fe after a brief period of Fe limitation (Fig. 2). It is noteworthy that the Fe- and Mn-accumulating conditions are distinct from those used in previous work. In contrast to the Cu-overaccumulating situation, the growth rate of the alga is not limited during Fe and Mn accumulation. For Fe in fact, the growth of the cells, which was initially Fe limited, improved dramatically by adding excess amounts of Fe. For Mn, a subtle but significant increase in growth rate was observed with higher Mn concentrations (figure 1A in ref. 47). The increase in intracellular Fe and Mn contents was solely driven by an increase in external (environmental) Fe or Mn. We suggest that the role of the acidocalcisome in these conditions is to sequester intracellularly unneeded (and hence excess) trace metals in order to maintain healthy Fe and Mn homeostasis in the cytoplasm.

We were able to quantitatively trace all intracellular metal pools using a combination of XFM and ICP-MS/MS. Vitrified and chemically fixed alga cells showed equally well correlation with bulk data. We found that up to 80% of total cellular Fe is stored in acidocalcisomes when cells are overaccumulating Fe. This means that almost all of the excess Fe, the amount that exceeds the native, replete Fe content in cells, is sequestered within the acidic vacuoles. The same is true in Zn-deficient conditions, where cells accumulate two to three times more Fe, and consequently up to 60% of total Fe can be found in acidocalcisomes, again reflecting the excess part of the Fe quota. This was confirmed by a quantitative analysis of the Fe concentrations inside the cells, but not sequestered within the vacuoles, where both Fe-accumulating conditions showed replete levels of Fe outside of storage compartments. This only leaves a limited role for other Fe storage sites in those conditions, for example the two ferritins Fer1 and Fer2 in *Chlamydomonas*. The abundance of the predominant plastid ferritin (Fer1) was shown to be reduced with increasing extracellular Fe availability (23, 27), which is more consistent with a role of ferritin in buffering Fe released from intracellular sources during times of Fe limitation (27). *Chlamydomonas* Fer2, which is also localized to the chloroplast and ~70-fold less abundant, was not reduced in abundance when Fe is more abundant in the medium, but also did not accumulate (23). Given the Fe distribution data (Fig. 2*B*), we did not note any accumulation of Fe in the chloroplast, leading us to conclude that Fer1 and 2 only have a minor role in Fe sequestration upon overaccumulation, if any. Many organisms in the Viridiplantae, which include chlorophyte algae and plants, harbor small gene families of ferritin, allowing for tissue-specific expression and regulation in response to different stimuli (64). In contrast to *Chlamydomonas*, ferritins in *Arabidopsis* and maize, for example, are induced upon exposure to elevated Fe and they do contribute to Fe storage (65, 66).

For Cu, the situation for storage is different. Lysosome-related organelles play a crucial role in Cu sequestration in eukaryotes, from yeast to mammals (67, 68). For example, storage and removal of excess Cu from liver hepatocytes is mediated via lysosomes (69); there Cu is associated with S, from metallothionein (70). Similar Cu concentrations (>80 mM) in areas of high Cu concentration have been observed in tumorous rat livers (71), although these areas of high Cu concentration were vastly bigger in size (>10 µm, compared with the <1 µm acidocalcisomes in *Chlamydomonas*). Additionally, in higher eukaryotes, Pushkar et al. identified Cu storage vesicles (CSVs) in astrocytes within the periventricular region of the lateral ventricle in rat and mouse brains (72). Cu concentrations within this compartment were also in a similar range to that observed here (100 to 300 mM). However, similar to liver cells, the sequestered Cu in

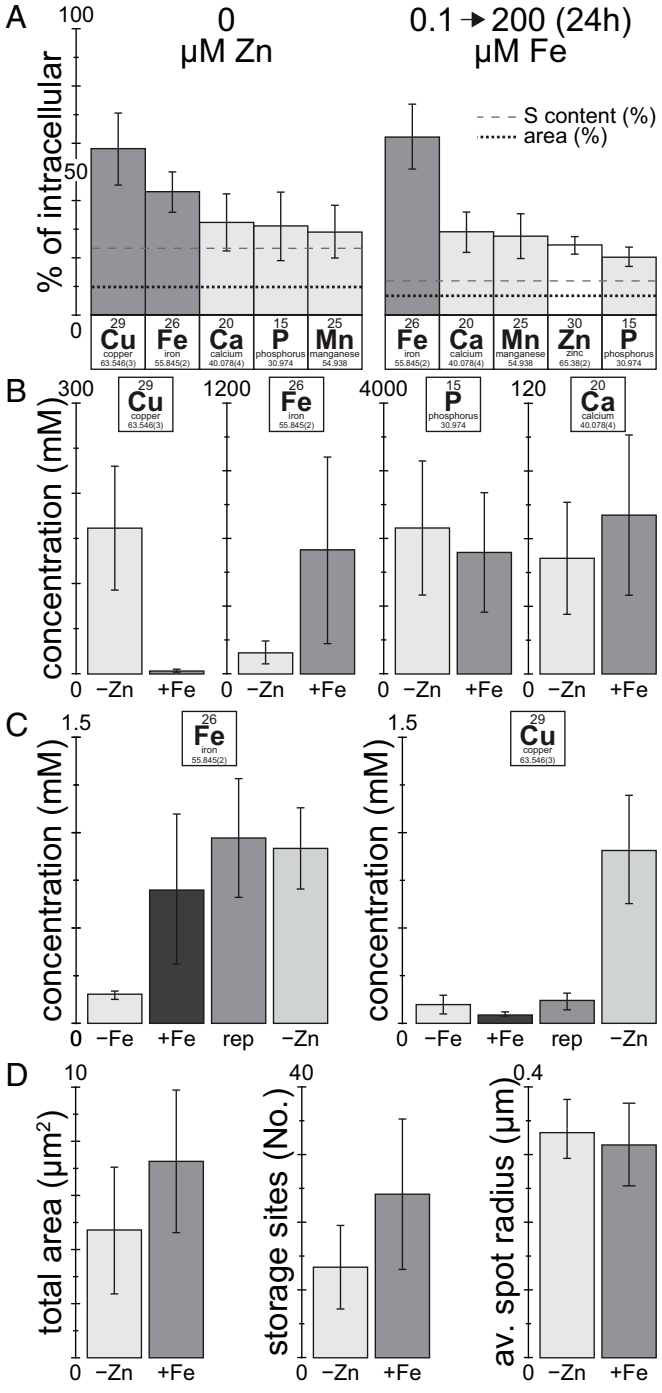

Fig. 5. Most of the Fe and Cu overload is in the acidocalcisome. (*A*) Fraction of total cellular elemental content enriched within areas of high Cu (in Zn deficiency) or high Fe content (in 24 h of Fe excess), respectively. Areas containing storage compartments were determined by a *k*-means clustering approach identifying areas of continuous, high Cu or Fe concentration, respectively, using the MAPS software. The black, dotted line indicates the fraction of the cell area containing storage compartments; the gray, dashed line indicates the fraction of the S content (as a proxy for the cell volume) within the areas containing storage compartments. Included are only elements enriched in the areas containing storage compartments. Error bars indicate SD from at least four individual cells. (*B*) Average Cu, Fe, Ca, and P concentration within the acidocalcisomes in Zn-deficiency (Cu-overaccumulation) or Fe-overaccumulating conditions. For calculation of the elemental concentration within the acidocalcisome, the volume of the organelle was extrapolated from the average dimensions obtained from the areas containing storage compartments, and the organelles were assumed to be spherical. Error bars indicate SD between organelles from at least four individual cells. (*C*) Average intracellular Fe and Cu concentration outside the storage regions, in replete, Fe-limited, Fe-overaccumulating and Zn-deficient conditions. Error bars indicate SD between at least four individual cells. (*D*) Total intracellular area containing storage compartments, the number of individual regions of continuous, high Cu or Fe concentration, and their extrapolated radius, derived from the total area covered and the number of regions within a cell. Error bars indicate SD between at least four individual cells.

astrocytes showed colocalization with S, probably from metallothionein, rather than with Ca or P. In *Chlamydomonas*, in both Zn-deficient and Fe-limited conditions, total Cu levels were elevated. The majority of Cu in Zn-deficient conditions is localized to acidocalcisomes (~55% on average, up to 70% in individual cells, Fig. 5), but that does not capture all of the excess intracellular Cu. Our findings suggest that at least 30% of the accumulating Cu in Zn deficiency is bound by different means, either proteins or small ligands. Additionally, in Fe-limited conditions, *Chlamydomonas* cells increase their Cu quota. This increase in Cu is of similar extent compared with the increase of Fe in Zn-deficient conditions (both increase two- to fourfold). While the increase in Fe can fully be explained by vacuolar Fe storage, for Cu, sequestration of the additional Cu in acidocalcisomes was not observed (Fig. 4*A*), suggesting other explanations for the higher cellular Cu quota. One possibility is that in Fe-limited cells Cu accumulates to serve physiological needs; for instance to accommodate elevated amounts of FOX1, a periplasmic multicopper oxidase involved in high-affinity Fe uptake. With 6 Cu atoms and dramatic up-regulation in Fe-limited cells, FOX1 can be a substantial (~12% of the quota) Cu-housing sink in the cell (14, 18, 73). Zn-deficient *Chlamydomonas* cells where *FOX1* expression also increases ~10-fold also have increased intracellular Cu outside the acidocalcisomes (Fig. 5*C*).

In summary, we utilized XFM to identify the acidocalcisomes as the storage site for Fe and Cu in situations of trace metal overaccumulation. We also quantified the elemental contents of whole cells and acidocalcisomes and are therefore able to distinguish the nutritional state of an alga at the level of a single cell. This is promising not only for trace metal distribution studies, but allows for comparative single cell work, since the technique is nondestructive. Combined with upcoming upgrades to XFM capacity, increasing either throughput or resolution, studies comparing the single-cell nutritional status with molecular indicators will be feasible.

Methods

Materials, Strains, and Culture Conditions. *C. reinhardtii* strains CC-4533 (CMJ030), CC-4425 (D66+), CC-5321 (*vtc1-1*) (43), CC-5324 (*VTC1-C2*, complemented *vtc1-1*) (43) were used for the experiments in this study. Cultures were cultivated in replete or trace metal-deficient medium, as indicated, in 250-mL Erlenmeyer flasks containing 100 mL TAP medium with a revised trace element solution, as described previously (74, 75). The cultures were grown with constant agitation in an Innova 44R incubator (160 rpm, New Brunswick Scientific) at 24 °C in continuous light (90 μmol m^{-2} s^{-1}), provided by cool white fluorescent bulbs (4,100 K) and warm white fluorescent bulbs (3,000 K) in the ratio of 2:1. All nutrient-deficient media were prepared in flasks that were treated with 6N hydrochloric acid (analytical grade) for at least 12 h, to reduce the trace metal background from the vessel and ensure accurate metal contents across replicates dependent on the addition of trace metals and not impurities. The acid-washed flasks were rinsed six times with Milli-Q water before use to remove traces of the acid. Single-use plastic serological pipettes and spatulas and similarly acid-washed graded cylinders were exclusively used during the preparation of any of the solutions in this study. Cu overaccumulation in Zn deficiency was achieved by subjecting replete *Chlamydomonas* cultures to two consecutive rounds of dilution to an initial concentration of 1×10^5 cells/mL, both times in medium that was prepared without the addition of Zn. Fe overaccumulation was achieved by diluting replete-grown, midlog *Chlamydomonas* cultures once to 1×10^4 cells/mL in 0.1 μM Fe media, before increasing the concentration in the culture to 200 μM Fe when the culture reached a

density of 1×10^6 cells/mL. The cell density reached between 3 and 6×10^6 cells/mL 24 h after the addition of Fe.

Total Nonpurgeable Carbon and Total Nitrogen Content Analysis. Total, nonpurgeable organic carbon content (NPOC) of the cells was determined as described in ref. 76 with minor modifications on a total organic carbon and total nitrogen analyzer (Shimadzu TOC-L/TN CSH). In brief, 3×10^7 cells were collected by centrifugation at 3,100 × *g* for 3 min, briefly washed once in 10 mM Na-phosphate (pH 7.0), and then resuspended in 900 μL of 3 M HCl (3.33×10^7 cells/mL). Cells in HCl were incubated for 16 h at 65 °C with constant agitation before being subjected to nonpurgeable organic C and total N analysis. The acidified samples were diluted to 3×10^5 cells/mL with Milli-Q water before being cleared of inorganic C by sparging with purified air and the determination of the NPOC and total nitrogen (TN) content. Each sample was measured at least three times with a nondispersive infrared gas analyzer (CO_2) and a chemiluminescence gas analyzer (TN). The peak area was calculated and compared with a standard curve from 0.5 to 25 ppm C (from potassium hydrogen phthalate) or N (from potassium nitrate) using the TOC-Control L software version 1.0 (Shimadzu). Measured concentrations did not exceed the calibration range and did not exceed 5% relative SD between the individual technical replicates.

Quantitative Trace Metal, S, and P Composition Analysis. The trace metal, S, and P composition was determined by ICP-MS/MS as described (77) with minor modifications. In brief, 5×10^7 *Chlamydomonas* cells of a culture during logarithmic growth phase (at a cell density between 1 and 5×10^6 cells/mL) were collected by centrifugation at 3,100 × *g* for 3 min in a 50-mL Falcon tube. The cells were washed three times in 1 mM disodium ethylenediaminetetraacetic acid (Na_2-EDTA), pH 8 (to remove cell surface-associated metals), and once in Milli-Q water (to remove the Na_2-EDTA) and transferred into a 15-mL Falcon tube in the process. The cell pellet, after removing the water, was overlaid with 143 μL of 70% nitric acid (trace metal grade, A467-500, Fisher Scientific) and incubated first at room temperature for 24 h and then at 65 °C for 4 h before being diluted to a final nitric acid concentration of 2% (vol/vol) with Milli-Q water. Aliquots of fresh or spent culture medium were treated with nitric acid to a final concentration of 2% (vol/vol). Metal, S, and P contents were determined on an Agilent 8800 Triple Quadrupole ICP-MS/MS instrument, in comparison with an environmental calibration standard (Agilent 5183-4688), a S (Inorganic Ventures CGS1) and P (Inorganic Ventures CGP1) standard, using ^{89}Y as an internal standard (Inorganic Ventures MSY-100PPM). The levels of all analytes were determined in MS/MS mode, where ^{39}K, ^{40}Ca, ^{56}Fe, and ^{78}Se were directly determined using H_2 as a cell gas, ^{23}Na, ^{24}Mg, ^{55}Mn, ^{59}Co, ^{60}Ni, ^{63}Cu, ^{66}Zn, and ^{95}Mo where directly measured using He as a cell gas, while ^{31}P and ^{32}S were determined via mass shift from 31 to 47 and 32 to 48, respectively, utilizing O_2 in the collision/reaction cell. The average of four to five technical replicate measurements was used for each individual biological sample. The average variation in between the technical replicate measurements was below 2% for all individual experiments and never exceeded 5% for an individual sample.

XFM. A total of 3×10^6 *Chlamydomonas* cells of a culture during logarithmic growth phase (at a cell density between 1 and 5×10^6 cells/mL) were collected by centrifugation at 16,100 × *g* at room temperature for 15 s in a 1.5-mL Eppendorf tube. The cell pellet was washed twice in 1 × phosphate-buffered saline (PBS) buffer (137 mM NaCl, 2.7 mM KCl, 10 mM Na_2HPO_4, 1.8 mM KH_2PO_4) and resuspended either in 0.3 mL Milli-Q water for vitrification or 4% paraformaldehyde (EM grade #15710 from EMS) in 1× PBS for chemical fixation. A total of 100 μL of the cell suspension was then applied to a poly-L-lysine-coated silicon nitride membrane window ($5 \times 5 \times 0.2$ mm frame, $2 \times 2 \times 0.0005$ mm Si_3N_4 membrane, Silson) and allowed to settle for 30 min at room temperature. After the supernatant was removed by gentle suction, the window was either directly mounted into an FEI Vitrobot Mark IV freezer for vitrification in liquid ethane (blot time 3 s, blot force 2, blot total 1, wait and drain time 0 s) or washed twice with 1× PBS, fresh 0.1 M ammonium acetate, and Milli-Q water. Windows with chemically fixed cells were air dried and stored at room temperature, windows with vitrified cells were kept in liquid nitrogen storage until measurement at low temperatures. The data presented here are from four individual sessions (48- to 72-h measurement time each) at the Bionanoprobe (46), over a period of 2 y, during which the analyzer was localized either at beamline 21-ID-D or beamline 9-ID-B at the Advanced Photon Source (APS) of the Argonne National Laboratory. Direct excitation of atomic K transitions was aimed for by tuning the incident X-ray energy to 10 keV, which allows efficient excitation of elements in the elemental table up to Zn (z = 30). Individual, large *Chlamydomonas* cells can be up to 15 μm in diameter before division, which is well below the 50 to 100 μm that can be penetrated by XFM with high-spatial resolution (51). Whole cells where therefore analyzed without sectioning. Two rounds of coarse scans were performed to identify cell locations on the SiN windows, with a pixel size between 0.5 and 2 μm in *x* and *y* directions. Then, a high-resolution scan of the individual cells was initiated for all images; a spatial resolution between 60 and 80 nm with a dwell time of 200 to 300 ms per pixel was used. With an average scan area of 10×10 μm, this results in measurement times up to 3 h per cell for each high resolution. By normalizing the recorded fluorescent spectrum with data obtained from a calibration standard, fully quantitative maps of the elemental distribution are obtained for each of the individual elements.

Data Analysis and Software. X-ray fluorescence data were fitted and analyzed using the MAPS software package (63). Exported images were further edited and assembled in Adobe Photoshop and Illustrator.

For the quantitative analysis, we defined three areas in the images, "whole cells," which were further divided into "areas containing storage compartments" and "intracellular areas outside of storage regions." Areas containing storage compartments, in all cases, were contained within the boundaries of the cells. The borders for the whole cells were identified in the images in the outside panels (Figs. 1–3) and were manually replicated in the MAPS software in order to determine the amount of all the material contained within the cells and the area that the cell covers. These data were used for comparisons with ICP MS/MS data (Fig. 4) of elemental content and contributed to the quantitative description of the metal storage compartment (Fig. 5). Areas containing storage compartments were determined automatically, as continuous areas of high Cu concentration in Zn deficiency or Fe concentration during Fe accumulation, respectively, using a *k*-means clustering approach within the MAPS software, in order to determine the total amounts of elements contained within these areas and the fraction of the cell that they cover. Intracellular areas outside of storage regions were defined as the areas within the boundaries of the cell, that did not have a high Cu or Fe content, respectively. They were identified as the inverse intracellular areas of the areas containing storage compartments.

Enrichment of elements within storage compartments (Fig. 5*A*) was determined with two criteria. Elements within storage compartments were required to accumulate to significantly greater levels than they would naturally, given the total cellular content of the element and the fraction of the area of the cell that contains storage compartments. A total of 9.9 (±3.8) % and 6.6 (±1.3) % of the area of the cell, on average, contained high concentrations of Cu or Fe, respectively, and therefore were considered to contain storage compartments. This fraction of the cell (average) is also presented by a black, dotted line in Fig. 5*A*. The average and SD of the fraction of the area containing storage compartments between individual cells, as well as the average and SD of the fraction of the elemental content in areas containing storage compartments between individual cells was used for the statistical analysis. However, there might be a bias for areas in the center of the cell, where the cells' thickness is highest, to show enrichment for individual elements. We therefore also required individual elements to exceed the abundance of S in these areas, which was the element within our analysis that best correlated with biomass, and is most equally distributed throughout the cells (*SI Appendix*, Figs. S2, S5, and S6). Therefore, within the parameters of the experiment, S distribution should best approximate the volume. The average S content in the areas containing storage compartments was determined between individual cells and was added to Fig. 5*A* as a dashed line. In the areas that have high Fe/Cu content, we found between 12 and 23% of the total cellular S. We recognize that this approach could be overly conservative with respect to identification of other elements, including S, that may be enriched within the storage organelles. But given the two-dimensional limitations of the methodology, we aimed to raise the bar for elements to be considered sequestered. The intracellular areas outside of storage regions were used to determine the intracellular concentration of Fe and Cu outside of the storage organelles (Fig. 5*C*).

In addition to the content of the different areas within the cell, the number of storage compartments/cell was determined manually by counting individual secluded areas within the cells. This number, together with the total area containing storage compartments, was used to determine the average dimensions (area and radius) of the storage compartments within individual cells (Fig. 5*D*).

Data Availability. All study data are included in the article and/or *SI Appendix*.

ACKNOWLEDGMENTS. This work was supported by a grant from the NIH (GM42143) to S.S.M. for the work on Cu, and by a grant from the Department

of Energy (DE-SC0020627) to S.S.M. and S.S. for the work on Fe. This research used resources from the Advanced Photon Source, a US Department of Energy (DOE) Office of Science User Facility, operated for the DOE Office of Science by Argonne National Laboratory under Contract No. DE-AC02-06CH11357. We appreciate the support of Keith Brister and Michael Bolbat at beamline 21-ID-D and the support of Evan Maxey at beamline 9-ID-B of the APS.

1. E. Andresen, E. Peiter, H. Küpper, Trace metal metabolism in plants. *J. Exp. Bot.* **69**, 909–954 (2018).
2. S. S. Merchant, The elements of plant micronutrients. *Plant Physiol.* **154**, 512–515 (2010).
3. C. Andreini, I. Bertini, G. Cavallaro, G. L. Holliday, J. M. Thornton, Metal ions in biological catalysis: From enzyme databases to general principles. *J. Biol. Inorg. Chem.* **13**, 1205–1218 (2008).
4. K. J. Waldron, J. C. Rutherford, D. Ford, N. J. Robinson, Metalloproteins and metal sensing. *Nature* **460**, 823–830 (2009).
5. T. Dudev, C. Lim, Competition among metal ions for protein binding sites: Determinants of metal ion selectivity in proteins. *Chem. Rev.* **114**, 538–556 (2014).
6. A. W. Foster, D. Osman, N. J. Robinson, Metal preferences and metallation. *J. Biol. Chem.* **289**, 28095–28103 (2014).
7. J. A. Cotruvo Jr, J. Stubbe, Metallation and mismetallation of iron and manganese proteins *in vitro* and *in vivo*: The class I ribonucleotide reductases as a case study. *Metallomics* **4**, 1020–1036 (2012).
8. J. A. Imlay, The mismetallation of enzymes during oxidative stress. *J. Biol. Chem.* **289**, 28121–28128 (2014).
9. J. A. Imlay, Cellular defenses against superoxide and hydrogen peroxide. *Annu. Rev. Biochem.* **77**, 755–776 (2008).
10. D. A. Capdevila, K. A. Edmonds, D. P. Giedroc, Metallochaperones and metalloregulation in bacteria. *Essays Biochem.* **61**, 177–200 (2017).
11. A. C. Rosenzweig, Metallochaperones: Bind and deliver. *Chem. Biol.* **9**, 673–677 (2002).
12. P. A. Salomé, S. S. Merchant, A series of fortunate events: Introducing Chlamydomonas as a reference organism. *Plant Cell* **31**, 1682–1707 (2019).
13. M. D. Allen, J. A. del Campo, J. Kropat, S. S. Merchant, *FEA1, FEA2*, and *FRE1*, encoding two homologous secreted proteins and a candidate ferrireductase, are expressed coordinately with *FOX1* and *FTR1* in iron-deficient *Chlamydomonas reinhardtii*. *Eukaryot. Cell* **6**, 1841–1852 (2007).
14. S. La Fontaine *et al*., Copper-dependent iron assimilation pathway in the model photosynthetic eukaryote *Chlamydomonas reinhardtii*. *Eukaryot. Cell* **1**, 736–757 (2002).
15. D. Malasarn *et al*., Zinc deficiency impacts CO_2 assimilation and disrupts copper homeostasis in *Chlamydomonas reinhardtii*. *J. Biol. Chem.* **288**, 10672–10683 (2013).
16. M. Castruita *et al*., Systems biology approach in *Chlamydomonas* reveals connections between copper nutrition and multiple metabolic steps. *Plant Cell* **23**, 1273–1292 (2011).
17. E. I. Urzica *et al*., Systems and *trans*-system level analysis identifies conserved iron deficiency responses in the plant lineage. *Plant Cell* **24**, 3921–3948 (2012).
18. J. Kropat *et al*., Copper economy in Chlamydomonas: Prioritized allocation and reallocation of copper to respiration vs. photosynthesis. *Proc. Natl. Acad. Sci. U.S.A.* **112**, 2644–2651 (2015).
19. M. D. Page *et al*., Fe sparing and Fe recycling contribute to increased superoxide dismutase capacity in iron-starved *Chlamydomonas reinhardtii*. *Plant Cell* **24**, 2649–2665 (2012).
20. S. Merchant, L. Bogorad, Regulation by copper of the expression of plastocyanin and cytochrome c_{552} in *Chlamydomonas reinhardi*. *Mol. Cell. Biol.* **6**, 462–469 (1986).
21. J. Moseley, J. Quinn, M. Eriksson, S. Merchant, The *Crd1* gene encodes a putative di-iron enzyme required for photosystem I accumulation in copper deficiency and hypoxia in *Chlamydomonas reinhardtii*. *EMBO J.* **19**, 2139–2151 (2000).
22. C. E. Blaby-Haas, S. S. Merchant, Regulating cellular trace metal economy in algae. *Curr. Opin. Plant Biol.* **39**, 88–96 (2017).
23. J. C. Long, F. Sommer, M. D. Allen, S. F. Lu, S. S. Merchant, *FER1* and *FER2* encoding two ferritin complexes *in Chlamydomonas reinhardtii* chloroplasts are regulated by iron. *Genetics* **179**, 137–147 (2008).
24. A. Hong-Hermesdorf *et al*., Subcellular metal imaging identifies dynamic sites of Cu accumulation in *Chlamydomonas*. *Nat. Chem. Biol.* **10**, 1034–1042 (2014).
25. A. M. Koorts, M. Viljoen, Ferritin and ferritin isoforms I: Structure-function relationships, synthesis, degradation and secretion. *Arch. Physiol. Biochem.* **113**, 30–54 (2007).
26. E. C. Theil, Ferritin protein nanocages use ion channels, catalytic sites, and nucleation channels to manage iron/oxygen chemistry. *Curr. Opin. Chem. Biol.* **15**, 304–311 (2011).
27. A. Busch, B. Rimbauld, B. Naumann, S. Rensch, M. Hippler, Ferritin is required for rapid remodeling of the photosynthetic apparatus and minimizes photo-oxidative stress in response to iron availability in *Chlamydomonas reinhardtii*. *Plant J.* **55**, 201–211 (2008).
28. C. Simm *et al*., *Saccharomyces cerevisiae* vacuole in zinc storage and intracellular zinc distribution. *Eukaryot. Cell* **6**, 1166–1177 (2007).
29. M. S. Szczypka, Z. Zhu, P. Silar, D. J. Thiele, *Saccharomyces cerevisiae* mutants altered in vacuole function are defective in copper detoxification and iron-responsive gene transcription. *Yeast* **13**, 1423–1435 (1997).
30. S. C. Li, P. M. Kane, The yeast lysosome-like vacuole: Endpoint and crossroads. *Biochim. Biophys. Acta* **1793**, 650–663 (2009).
31. J. L. Urbanowski, R. C. Piper, The iron transporter Fth1p forms a complex with the Fet5 iron oxidase and resides on the vacuolar membrane. *J. Biol. Chem.* **274**, 38061–38070 (1999).
32. S. Thomine, F. Lelièvre, E. Debarbieux, J. I. Schroeder, H. Barbier-Brygoo, AtNRAMP3, a multispecific vacuolar metal transporter involved in plant responses to iron deficiency. *Plant J.* **34**, 685–695 (2003).
33. H. C. Roh, S. Collier, J. Guthrie, J. D. Robertson, K. Kornfeld, Lysosome-related organelles in intestinal cells are a zinc storage site in *C. elegans*. *Cell Metab.* **15**, 88–99 (2012).
34. S. Thomine, G. Vert, Iron transport in plants: Better be safe than sorry. *Curr. Opin. Plant Biol.* **16**, 322–327 (2013).
35. K. Komsic-Buchmann, L. Wöstehoff, B. Becker, The contractile vacuole as a key regulator of cellular water flow in *Chlamydomonas reinhardtii*. *Eukaryot. Cell* **13**, 1421–1430 (2014).
36. P. Luykx, M. Hoppenrath, D. G. Robinson, Structure and behavior of contractile vacuoles in*Chlamydomonas reinhardtii*. *Protoplasma* **198**, 73–84 (1997).
37. F. Xu, X. Wu, L. H. Jiang, H. Zhao, J. Pan, An organelle K+ channel is required for osmoregulation in *Chlamydomonas reinhardtii*. *J. Cell Sci.* **129**, 3008–3014 (2016).
38. R. Docampo, W. de Souza, K. Miranda, P. Rohloff, S. N. Moreno, Acidocalcisomes–Conserved from bacteria to man. *Nat. Rev. Microbiol.* **3**, 251–261 (2005).
39. A. E. Vercesi, S. N. Moreno, R. Docampo, Ca^{2+}/H^+ exchange in acidic vacuoles of *Trypanosoma brucei*. *Biochem. J.* **304**, 227–233 (1994).
40. J. Deng *et al*., Simultaneous cryo X-ray ptychographic and fluorescence microscopy of green algae. *Proc. Natl. Acad. Sci. U.S.A.* **112**, 2314–2319 (2015).
41. J. Deng *et al*., X-ray ptychographic and fluorescence microscopy of frozen-hydrated cells using continuous scanning. *Sci. Rep.* **7**, 445 (2017).
42. R. Docampo, G. Huang, Acidocalcisomes of eukaryotes. *Curr. Opin. Cell Biol.* **41**, 66–72 (2016).
43. M. Aksoy, W. Pootakham, A. R. Grossman, Critical function of a *Chlamydomonas reinhardtii* putative polyphosphate polymerase subunit during nutrient deprivation. *Plant Cell* **26**, 4214–4229 (2014).
44. U. Goodenough, A. A. Heiss, R. Roth, J. Rusch, J. H. Lee, Acidocalcisomes: Ultrastructure, biogenesis, and distribution in microbial eukaryotes. *Protist* **170**, 287–313 (2019).
45. C. M. Ackerman, S. Lee, C. J. Chang, Analytical methods for imaging metals in biology: From transition metal metabolism to transition metal signaling. *Anal. Chem.* **89**, 22–41 (2017).
46. S. Chen *et al*., The Bionanoprobe: Hard X-ray fluorescence nanoprobe with cryogenic capabilities. *J. Synchrotron Radiat.* **21**, 66–75 (2014).
47. M. Tsednee *et al*., Manganese co-localizes with calcium and phosphorus in *Chlamydomonas* acidocalcisomes and is mobilized in manganese-deficient conditions. *J. Biol. Chem.* **294**, 17626–17641 (2019).
48. T. Paunesku, S. Vogt, J. Maser, B. Lai, G. Woloschak, X-ray fluorescence microprobe imaging in biology and medicine. *J. Cell. Biochem.* **99**, 1489–1502 (2006).
49. R. Ortega, G. Devès, A. Carmona, Bio-metals imaging and speciation in cells using proton and synchrotron radiation X-ray microspectroscopy. *J. R. Soc. Interface* **6** (suppl. 5), S649–S658 (2009).
50. S. C. Leary, M. Ralle, Advances in visualization of copper in mammalian systems using X-ray fluorescence microscopy. *Curr. Opin. Chem. Biol.* **55**, 19–25 (2020).
51. D. Wagner *et al*., Elemental analysis of *Mycobacterium avium*-, *Mycobacterium tuberculosis*-, and *Mycobacterium smegmatis*-containing phagosomes indicates pathogen-induced microenvironments within the host cell's endosomal system. *J. Immunol.* **174**, 1491–1500 (2005).
52. D. Glesne, S. Vogt, J. Maser, D. Legnini, E. Huberman, Regulatory properties and cellular redistribution of zinc during macrophage differentiation of human leukemia cells. *J. Struct. Biol.* **155**, 2–11 (2006).
53. L. Finney *et al*., X-ray fluorescence microscopy reveals large-scale relocalization and extracellular translocation of cellular copper during angiogenesis. *Proc. Natl. Acad. Sci. U.S.A.* **104**, 2247–2252 (2007).
54. A. Cohen, N. Perzov, H. Nelson, N. Nelson, A novel family of yeast chaperons involved in the distribution of V-ATPase and other membrane proteins. *J. Biol. Chem.* **274**, 26885–26893 (1999).
55. O. Müller *et al*., The Vtc proteins in vacuole fusion: Coupling NSF activity to $V(_0)$ *trans*-complex formation. *EMBO J.* **21**, 259–269 (2002).
56. M. Hothorn *et al*., Catalytic core of a membrane-associated eukaryotic polyphosphate polymerase. *Science* **324**, 513–516 (2009).
57. N. Ogawa, J. DeRisi, P. O. Brown, New components of a system for phosphate accumulation and polyphosphate metabolism in *Saccharomyces cerevisiae* revealed by genomic expression analysis. *Mol. Biol. Cell* **11**, 4309–4321 (2000).
58. S. H. Klompmaker, K. Kohl, N. Fasel, A. Mayer, Magnesium uptake by connecting fluid-phase endocytosis to an intracellular inorganic cation filter. *Nat. Commun.* **8**, 1879 (2017).
59. D. Mustafi *et al*., X-ray fluorescence microscopy demonstrates preferential accumulation of a vanadium-based magnetic resonance imaging contrast agent in murine colonic tumors. *Mol. Imaging* **14**, 1–12 (2015).
60. T. Paunesku *et al*., X-ray fluorescence microscopy for investigation of archival tissues. *Health Phys.* **103**, 181–186 (2012).
61. L. Balcaen, G. Woods, M. Resano, F. Vanhaecke, Accurate determination of S in organic matrices using isotope dilution ICP-MS/MS. *J. Anal. At. Spectrom.* **28**, 33–39 (2013).
62. S. Diez Fernández, N. Sugishama, J. Ruiz Encinar, A. Sanz-Medel, Triple quad ICPMS (ICPQQQ) as a new tool for absolute quantitative proteomics and phosphoproteomics. *Anal. Chem.* **84**, 5851–5857 (2012).

63. S. Vogt, MAPS: A set of software tools for analysis and visualization of 3D X-ray fluorescence data sets. *J. Phys. IV France* **104**, 635–638 (2003).
64. J. F. Briat *et al*., New insights into ferritin synthesis and function highlight a link between iron homeostasis and oxidative stress in plants. *Ann. Bot.* **105**, 811–822 (2010).
65. I. Fobis-Loisy, K. Loridon, S. Lobréaux, M. Lebrun, J. F. Briat, Structure and differential expression of two maize ferritin genes in response to iron and abscisic acid. *Eur. J. Biochem.* **231**, 609–619 (1995).
66. J. M. Petit, J. F. Briat, S. Lobréaux, Structure and differential expression of the four members of the *Arabidopsis thaliana* ferritin gene family. *Biochem. J.* **359**, 575–582 (2001).
67. T. Nevitt, H. Öhrvik, D. J. Thiele, Charting the travels of copper in eukaryotes from yeast to mammals. *Biochim. Biophys. Acta* **1823**, 1580–1593 (2012).
68. C. E. Blaby-Haas, S. S. Merchant, Lysosome-related organelles as mediators of metal homeostasis. *J. Biol. Chem.* **289**, 28129–28136 (2014).
69. J. B. Gross Jr., B. M. Myers, L. J. Kost, S. M. Kuntz, N. F. LaRusso, Biliary copper excretion by hepatocyte lysosomes in the rat. Major excretory pathway in experimental copper overload. *J. Clin. Invest.* **83**, 30–39 (1989).
70. D. Klein *et al*., Association of copper to metallothionein in hepatic lysosomes of Long-Evans cinnamon (LEC) rats during the development of hepatitis [se e comments]. *Eur. J. Clin. Invest.* **28**, 302–310 (1998).
71. C. I. Davis *et al*., Altered copper homeostasis underlies sensitivity of hepatocellular carcinoma to copper chelation. *Metallomics* **12**, 1995–2008 (2020).
72. Y. Pushkar *et al*., Aging results in copper accumulations in glial fibrillary acidic protein-positive cells in the subventricular zone. *Aging Cell* **12**, 823–832 (2013).
73. S. S. Merchant, S. Schmollinger, D. Strenkert, J. L. Moseley, C. E. Blaby-Haas, From economy to luxury: Copper homeostasis in Chlamydomonas and other algae. *Biochim. Biophys. Acta Mol. Cell Res.* **1867**, 118822 (2020).
74. J. Kropat *et al*., A revised mineral nutrient supplement increases biomass and growth rate in *Chlamydomonas reinhardtii*. *Plant J.* **66**, 770–780 (2011).
75. E. Harris, *The Chlamydomonas Sourcebook: A Comprehensive Guide to Biology and Laboratory Use* (Academic Press, Inc., 1989).
76. S. Schmollinger *et al*., Nitrogen-sparing mechanisms in *Chlamydomonas* affect the transcriptome, the proteome, and photosynthetic metabolism. *Plant Cell* **26**, 1410–1435 (2014).
77. D. Strenkert *et al*., Genetically programmed changes in photosynthetic cofactor metabolism in copper-deficient *Chlamydomonas*. *J. Biol. Chem.* **291**, 19118–19131 (2016).